Redox and Functional Analysis of the Rieske Ferredoxin Component of the Toluene 4-Monooxygenase[†]

Nathaniel L. Elsen, Luke A. Moe, Lea A. McMartin, and Brian G. Fox*

Department of Biochemistry and Center for Eukaryotic Structural Genomics, College of Agricultural and Life Sciences, University of Wisconsin, Madison, Wisconsin 53706-1544

Received August 8, 2006; Revised Manuscript Received October 17, 2006

ABSTRACT: Toluene 4-monooxygenase catalyzes the NADH- and O_2-dependent hydroxylation of toluene to form *p*-cresol. The four-protein complex consists of a diiron hydroxylase, an oxidoreductase, a catalytic effector protein, and a Rieske-type ferredoxin (T4moC). Phylogenetic analysis suggests that T4moC is part of a clade specialized for reaction with diiron hydroxylases, possibly reflected in the conservation of W69, whose indole side chain makes close contacts with a bridging sulfide. In order to further investigate the possible origins of this specialization, T4moC, mutated variants of T4moC, and three other purified ferredoxins (the *Thermus* Rieske protein, the *Burkeholderia cepacia* Rieske-type biphenyl dioxygenase ferredoxin BphF, and the *Ralstonia pickettii* PK01 toluene monooxygenase TbuB, the Rieske-type ferredoxin from another diiron monooxygenase complex) were studied by redox potential measurements and their ability to complement the catalytic function of the reconstituted toluene 4-monooxygenase complex. A saturation mutagenesis of T4moC W69 indicates that an aromatic residue may modulate the redox potential and is also necessary for activity and/or stability. The redox potential of T4moC was determined to be −173 mV, W69F T4moC was −139 mV, and TbuB was −150 mV. For comparison, BphF had a redox potential of −157 mV [Couture et al. (2001) *Biochemistry 40*, 84−92]. Of these ferredoxins, all except BphF were able to provide catalytic activity. Given the range in redox potentials observed in the active ferredoxins, shape and electrostatics are strongly implicated in the catalytic specialization. Mutagenesis of other T4moC surface residues gave further insight into possible origins of catalytic specialization. Thus R65A T4moC gave an alteration in apparent K_M only, while D82A/D83A T4moC gave alterations in both apparent k_{cat} and K_M. Since the different catalytic results were obtained by mutagenesis of residues lying on different sides of the protein adjacent to the [2Fe-2S] cluster, the results suggest that two different faces of T4moC may be involved in protein−protein interactions during catalysis.

The ability of ferredoxins to recognize specific protein partners inside the cell is a matter of considerable fascination (*1*−*3*). The basis for how proteins with highly homologous structures may exhibit nearly exclusive specificity for their cognate electron transfer partners has many contributions, starting with gene organization, cellular compartmentalization, and iron−sulfur cluster assembly (*4*). Other molecular determinants of the specificity include molecular shape, electrostatic complementarity, and thermodynamics, manifested in the separation of redox potentials between electron donor and acceptor (*5*).

In this work, we have examined the contribution of a specialized Rieske-type ferredoxin to the function of the four-protein toluene 4-monooxygenase (T4MO)[1] complex. Rieske proteins and Rieske-type ferredoxins are widely distributed and structurally well characterized (*6*−*14*). They have a conserved fold topology primarily composed of β-sheet (*8*, *15*−*21*) and a characteristic metal-binding motif of CXH and CXXH separated by 15−21 amino acids. Among the proteins referenced above, the Rieske-type ferredoxins from certain bacterial monooxygenase (*13*) and dioxygenase (*15*, *19*) complexes act as soluble electron carriers to mediate electron transfer between a flavin NAD(P)H oxidoreductase and a non-heme iron enzyme that is the terminal electron acceptor and contains the catalytic active site. Phylogenetic analyses suggest that, although originally related, the Rieske-type ferredoxins from the monooxygenase and dioxygenase complexes have evolved into two separate clades specialized for reaction with their different enzyme complexes (*13*, *19*, *22*). Therefore, in light of the structural homology observed for the Rieske-type ferredoxins, it is relevant to consider how the specialization for interaction with different electron transfer partners might arise.

The T4MO enzyme complex catalyzes the NADH- and O_2-dependent hydroxylation of toluene to form *p*-cresol (*23*, *24*). The complex consists of an NADH oxidoreductase (T4moF), a catalytic effector protein (T4moD), a diiron hydroxylase (T4moH), and a 112 amino acid Rieske-type

[†] This work was funded by National Science Foundation Grant MCB-0316232 (to B.G.F.).

* To whom correspondence should be addressed: phone, (608) 262-9708; fax, (608) 262-3453; e-mail, bgfox@biochem.wisc.edu.

[1] Abbreviations: T4MO, four-protein toluene 4-monooxygenase complex from *Pseudomonas mendocina* KR1; T4moH, hydroxylase component of T4MO; T4moC, Rieske-type [2Fe-2S] component of T4MO; TbuB, Rieske-type ferredoxin of the toluene monooxygenase complex from *Ralstonia pickettii* PK01; BphF, Rieske-type ferredoxin of the biphenyl dioxygenase complex from *Burkeholderia cepacia* strain LB400; Tt, Rieske protein from *Thermus thermophilus*.

10.1021/bi0616145 CCC: $37.00
Published on Web 01/06/2007

ferredoxin (T4moC). T4moC is a soluble monomeric ferredoxin that acts as an electron carrier between T4moF and T4moH, ultimately providing two electrons to the T4moH diiron cluster per catalytic turnover (*24*).

We have considered the basis for functional specialization in the T4MO complex by study of T4moC and three structural homologues: the *Thermus thermophilis* Rieske protein (Tt), the biphenyl dioxygenase ferredoxin (BphF), and the Rieske-type ferredoxin (TbuB) from *Ralstonia pickettii* PK01 toluene monooxygenase, another diiron monooxygenase. These four ferredoxins have redox potentials that span a range of >300 mV, vary substantially in their overall surface electrostatics, and, as demonstrated here, have profound differences in their ability to complement T4MO catalysis.

The results show that T4moC and TbuB have redox potentials similar to BphF (*25*). Given the similarity in reduction potentials, it is significant that only T4moC (*24*) and TbuB (*26*) were capable of reconstituting the T4MO catalytic reaction. This result strongly implicates shape and electrostatic complementarity in the catalytic specificity. A comparison of the X-ray structures of T4moC (*22*) and BphF (*15*) showed differences in a number of residues that were not ligands to the [2Fe-2S] cluster. Mutagenesis of nonligand residues conserved within the monooxygenase phylogenetic clade but not in the dioxygenase clade was used to further investigate the contributions of these residue positions to redox potential and specificity. The mutations investigated gave minor changes in the redox potential of T4moC but distinct effects on steady-state catalysis, depending on the surface of T4moC where the mutations were introduced. This introduces the possibility that local shape and electrostatic features modulate different protein−protein interactions involving T4moC and the other proteins of the T4MO complex. Furthermore, the results suggest a model where different faces of T4moC may also be specialized for optimal interactions with other proteins of the T4MO complex.

MATERIALS AND METHODS

Materials. Enzyme substrates, products, and other chemicals were from Aldrich (Milwaukee, WI). Vent DNA polymerase and restriction enzymes were from New England Biolabs (Beverly, MA). The QuikChange II site-directed mutagenesis kit, Turbo, and Yield Ace DNA polymerases were from Stratagene (La Jolla, CA). DNA extraction and purification kits were from Q-BIO (Carlsbad, CA) and Qiagen (Valencia, CA). *Escherichia coli* strains DH5α (Pharmacia, Piscataway, NJ) and NovaBlue and BL21(DE3) (Novagen, Madison, WI) were used for cloning and expression, respectively. PCR primers were from Integrated DNA Technologies, Inc. (Coralville, IA). Envirogen (Lawrenceville, NJ) provided a plasmid containing the *R. pickettii* PK01 toluene monooxygenase operon.

Preparation of T4moC and Mutated Isoforms. R65, D82, D83, C84, and C85 of T4moC were mutated to Ala as previously reported (*22*). Saturation mutagenesis of W69 was performed in a similar manner. The mutated plasmids were transformed into *E. coli* NovaBlue. The transformation mixture was plated onto Luria−Bertani plates supplemented with ampicillin (200 μg/mL) to obtain ∼200 individual colonies per 35 mm diameter agar plate. Individual isolates were evaluated for indole and toluene oxidation activity (*27*). Plasmid DNA was isolated from both indole-positive and negative clones for sequencing to determine the identity of mutations. DNA sequencing was done using the BigDye terminator mix (Applied Biosystems, Foster City, CA) at the University of Wisconsin Biotechnology Cluster. The genes encoding the W69F and W69A isoforms of T4moC were subcloned by PCR to include a 5′ *Nde*I site. The amplified fragment was digested with *Nde*I and *Blp*I and ligated into a similarly digested pET-15b derivative modified to be selectable by tetracycline. W69F C84A/C85A T4moC was created using overlap extension PCR to incorporate the W69F mutation into C84A/C85A T4moC. The expression and purification of T4moC and all isoforms described were as previously reported (*28*, *29*). The TbuB Rieske ferredoxin from the *R. pickettii* PKO1 toluene monoxygenase complex was cloned by PCR, expressed in *E. coli*, and purified using methods developed for T4moC.

Catalytic Assays. A unit of T4MO activity is defined as the formation of 1 μmol of *p*-cresol/min in air-saturated 50 mM phosphate buffer, pH 7.5 at 298 K, in the presence of optimal concentrations of the T4MO components, toluene-saturated buffer (5.8 mM at 298 K), and NADH (0.5 mM). The reconstitution of the purified T4MO complex and determination of catalytic activity were as previously described (*30*).

For determination of the product distribution from toluene, *E. coli* NovaBlue clones were grown overnight in Luria−Bertani medium supplemented with ampicillin (300 μg/mL) at 37 °C. After 12−15 h, 650 μL of the culture was used for catalytic assays, while the remainder was used for plasmid isolation. The 650 μL of culture was supplemented with 350 μL of an inducing solution containing α-lactose (8 mg/mL), casamino acids (2 mg/mL), ferrous sulfate (11 μg/mL), and ampicillin (300 μg/mL). The 1 mL culture was transferred to a sterile 17 × 100 mm culture tube, 0.5 μL of toluene was added directly into the induced culture, and the lid was snapped shut. After 2 h of shaking at 37 °C, an additional 1 μL of toluene was added, and the culture was allowed to shake for 2 h at 37 °C. The reaction was quenched by the addition of 100 μL of the culture to 50 μL of 2 M HCl saturated with NaCl. The products were extracted with 100 μL of chloroform containing 50 μM 3-methylbenzyl alcohol as an internal quantification standard. The activities of the individual isoforms were determined from total products as a percentage of the 3-methylbenzyl alcohol standard and compared to a similarly determined percentage observed from the natural enzyme.

Redox Titrations. Midpoint reduction potentials were determined by fixed potential redox titration in an argon-purged sample chamber as previously described (*31*). Ferredoxin (∼40 μM) was prepared in 150 mM MOPS, pH 7.0, and 200 mM KCl with 40 μM of the redox mediators duroquinone, 2-hydroxy-1,4-naphthoquinone, and anthraquinone-2-sulfonate. These redox mediators do not contribute substantial absorbance in either the oxidized or reduced states at 566 nm. Different fixed potentials were applied using an Epsilon EC potentiostat (Analytical Systems, West Lafayette, IN), and the current flow was monitored until the applied and system potentials were matched. The applied potential was removed, and the system potential was monitored for

~5 min until the change in potential was less than ~1 mV/min. The sample was then transferred to an airtight quartz cuvette filled with O_2-free argon, and the absorbance spectrum was obtained. The redox potentials of the mediators determined using the same titration device and buffer as used for the ferredoxin titrations were −144 and −216 mV, respectively, in close agreement with previously reported values (*32*, *33*).

For the final titration sample during ferredoxin reductions, the potentiostat was set to −500 mV, and the current was monitored until it was ~0.5% of the initial value. This sample (considered to be fully reduced) was immediately transferred to the airtight cuvette, and the absorbance spectrum was obtained. The extent of [2Fe-2S] reduction was calculated from the absorbance measured at 566 nm assuming $\epsilon_{566,ox} = 2.8\ mM^{-1}\ cm^{-1}$ and $\epsilon_{566,red} = 1.0\ mM^{-1}\ cm^{-1}$. The titration data were fit using eq 1, which is a transformation of the Nernst equation to express the percentage of oxidized Rieske ferredoxin present during the titration as a function of *n*, the number of electrons transferred, and the difference between *E*, the measured potential, and E_m, the calculated midpoint potential.

$$\%\ \text{oxidized} = \frac{100}{10^{-n(E-E_m)/59} + 1} \qquad (1)$$

Electronic Structure Calculations. The model of the Rieske cluster used for DFT calculations was based on coordinates from the X-ray crystal structure of T4moC, PDB code 1vm9 (*22*). Cysteine ligands to the [2Fe-2S] cluster were truncated to a single methyl group on the ligating sulfide, and histidine ligands were replaced with ammonia. The models used for Trp and Phe were indole and toluene, respectively. Geometry optimizations and single point DFT calculations were performed using the ORCA 2.4.02 software package (*34*). The Alrichs polarized split valence [SV(P)] basis (*34*) along with the SV/C auxiliary basis was used for all atoms with the exception of Fe, which were treated with the larger TZVP (triple-ζ valence polarization) basis (*35*). Becke's three-parameter hybrid functional for exchange (*36*) was used in combination with the Lee−Yang−Parr correlation functional (B3LYP/G) (*37*). Spin-unrestricted calculations were performed on the oxidized Rieske cluster, while spin-restricted calculations were performed on indole. The electron density and molecular orbitals were visualized with the gOpenMol program (*38*).

Other Analyses. The VAST website (http://www.ncbi.nlm.nih.gov/Structure/VAST/vastsearch.html) was used to identify structurally related proteins in the Molecular Modeling Database (*39*). A model of TbuB was built by threading onto the T4moC backbone with ESyPred3D (*40*) and the modeling package MODELLER. The [2Fe-2S] cluster was not included in the TbuB modeling; however, the conserved Cys and His side chains adopted appropriate conformations for ligation of the [2Fe-2S] cluster. The APBS program (*41*) and the Amber02 force field were used to calculate surface electrostatic potentials and total protein charge (*42*). The cysteine ligands were assigned the CYM residue type, the histidine ligands were assigned the HIE residue type [consistent with the protonation state assigned by NMR (*43*)], and a simple [2Fe-2S] cluster core was assigned consisting of two Fe^{3+} ions and two S^{2-} ions. The protein dielectric was 2 and the solvent dielectric was 80. Structures were aligned using align and pair_fit routines of PyMOL. Root-mean-squared deviations between solved structures were calculated using PyMOL.

RESULTS

Sequence Alignment. Figure 1 shows a structure-edited alignment of the sequences of the Rieske-type proteins discussed herein. All contain the CXH and CXXH metal-binding motif, and many contain a prolyl residue corresponding to P81 of T4moC. Of the proteins indicated in Figure 1, T4moC (*22*), BphF (*15*), and TbuB are the most closely related by their structural similarities and by their functional roles in multiprotein oxygenase complexes. In this alignment, the diiron hydroxylase ferredoxins (represented by T4moC and TbuB) have a tryptophan residue in the position corresponding to W69 of T4moC. The Rieske-type ferredoxin domain of naphthalene dioxygenase also has a tryptophan residue at this position, as shown for other members of the *cis*-diol-forming dioxygenase protein family by other alignments (*19*, *44*). However, BphF and other members of the biphenyl dioxygenase Rieske-type ferredoxin family (including structurally characterized carbazole 1,9a-dioxygenase ferredoxin) have glycine at this position, while the high-potential oxidase Rieske proteins have either serine or threonine.

Hydrogen Bonding to Rieske [2Fe-2S] Clusters. Site-directed mutagenesis (*45*, *46*) and computational studies (*47*) have shown that hydrogen bonding plays an important role in modulating the redox potential of the Rieske cluster. Residue positions marked with an "*h*" in Figure 1 are involved in hydrogen-bonding interactions of the [2Fe-2S] cluster in one or more of the Rieske ferredoxins. For these studies, we used criteria developed previously (*17*) to assign hydrogen bonding to an inorganic sulfide of the [2Fe-2S] cluster or SG of a ligating cysteine, i.e., a donor−acceptor distance less than 3.80 Å and a donor−proton−acceptor angle between 120° and 180° (*17*). A survey of structurally characterized Rieske proteins with known redox potentials established an ~+70 mV shift in redox potential for each backbone amide hydrogen bond donor and >+100 mV shift for a hydroxyl hydrogen bond donor (*17*). Thus the oxidase Rieske proteins and AO, with redox potentials ranging from +150 (*48*) to +490 mV (*49*), have the most hydrogen bonds to the cluster, including five or six amide and one or two hydroxyl hydrogen bond donors (*21*, *50*). The Rieske-type ferredoxin from carbazole 1,9a-dioxygenase from *Pseudomonas resinovorans* strain CA10 (*19*), with the lowest redox potential at −169 mV, has only two hydrogen bond donors from backbone amides that satisfy the criteria (*19*). The number of hydrogen bonds to the cluster of T4moC suggested that the redox potential might be ~0 mV by consideration of Figure 5 in the Supporting Information of ref *17*.

Table 1 summarizes the pattern and number of hydrogen bonds observed to the sulfur atoms of the Rieske cluster. At positions 1, 2, and 4, the high-potential Rieske protein, Tt, has two hydrogen bonds (*17*), from a combination of backbone amides and one side chain hydroxyl group. In contrast, T4moC has one hydrogen bond at position 1 (Cys64-SG) from Ala66-NH and one hydrogen bond at position 2 from Gln48-NH, while BphF retains one hydrogen

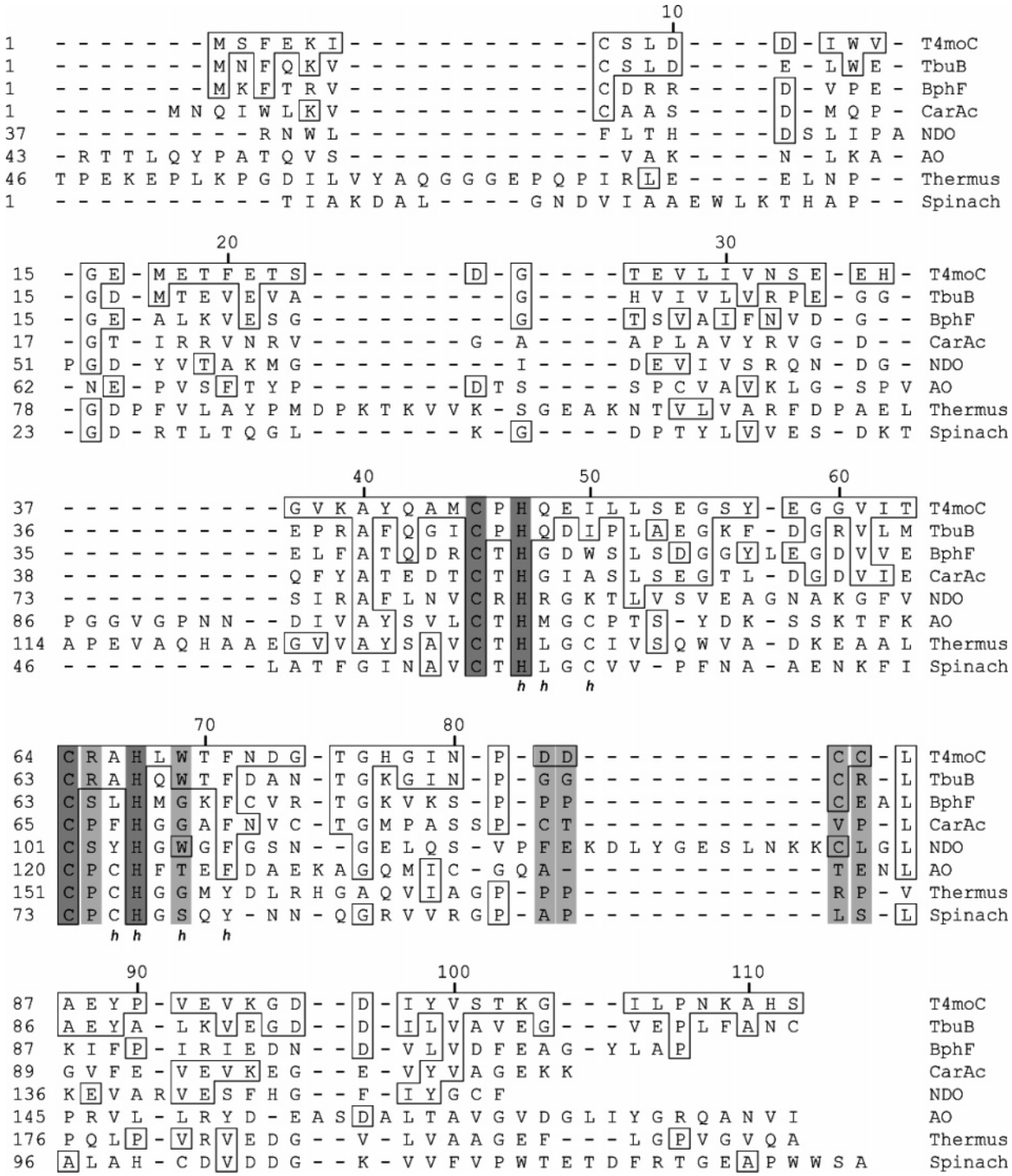

FIGURE 1: A structure-edited alignment of representative Rieske ferredoxin sequences. The primary sequence alignment obtained from ClustalW was modified to correspond to residue positions in loops observed in the aligned structures of each ferredoxin with T4moC. Cys and His residues acting as [2Fe-2S] cluster ligands are shown in dark gray. Residues mutated in this study are shown in light gray. Residue positions involved in hydrogen bonding to the [2Fe-2S] clusters of Rieske ferredoxins are marked with an "h".

bond to position 1 from Leu65-NH but lacks a hydrogen bond to position 2. At position 3 (Cys45-SG of T4moC), all of the representative Rieske protein structures (Tt, T4moC, BphF) have one hydrogen bond, provided by the amide NH of a histidine ligand (His47 in T4moC). At position 4, BphF has only one hydrogen bond, while T4moC and Tt have two hydrogen bonds. The additional hydrogen bond at position 4 in T4moC is provided by Trp69-NH. The indole ring of Trp69 is also in position for van der Waals contact to the bridging sulfide atom at position 4 (see below); the Rieske proteins in which the Pro loop is not displaced from the [2Fe-2S] cluster by an aromatic residue (BphF, Tt) do not have this possibility.

Redox Titrations. Figure 2 shows absorbance spectra obtained from a representative redox titration of T4moC in the presence of the redox mediators. At 566 nm, T4moC has an ϵ_{ox} of 2.8 mM^{-1} cm^{-1} and ϵ_{red} of 1.0 mM^{-1} cm^{-1}. Figure 3 shows representative least-squares fitting of the titration results using eq 1, and Table 2 shows the redox potentials determined from these titrations. The titration data were analyzed with $n = 1$, as expected for the redox reaction of a [2Fe-2S] cluster and, alternatively, with n allowed to

Table 1: Hydrogen-Bonding Interactions of the [2Fe-2S] Cluster in T4moC and Related Rieske Proteins

position in T4moC[a]	T4moC	BphF	Tt
1 Cys64-SG	Ala66-NH	Leu65-NH	C153-NH
2 μ-S	Gln48-NH		L135-NH
			C137-NH
3 Cys45-SG	His45-NH	His45-NH	His134-NH
			Tyr158-OH
4 μ-S	His67-NH	Gly68-NH	His154-NH
	Trp69-NH		Gly156-NH

[a] The comparable Cys residues in BphF are Cys43 and Cys63 and in Tt are Cys132 and Cys151.

float as a fitting parameter. When both n and E_m were allowed to vary as fitting parameters of eq 1, n remained close to 1 for all of the T4moC variants studied, and the calculated midpoint potentials were within the stated errors obtained with fixed $n = 1$. The redox potentials of T4moC (Figure 3A, Table 2) and C84A/C85A T4moC (Figure 3B, Table 2) were equivalent, with values of -173 ± 4 and -169 ± 6 mV, respectively. Thus the C84A/C85A mutations used to eliminate aggregation of T4moC during crystallization trials (*22*) had no influence on the redox potential (Table 2), which is in accord with the catalytic properties established for C84A/C85A T4moC (see Table 3). Table 2 also shows that the redox potential determined for W69F T4moC was -139 ± 3 mV and the potential of C83A TbuB was -150 ± 3 mV, representing $+30$ and $+19$ mV shifts relative to C84A/C85A T4moC. The redox potentials determined for other T4moC variants are also shown in Table 2.

After complete reduction of C84A/C85A T4moC, air was admitted into the cuvette in order to oxidize the sample. The optical spectrum of the air-oxidized protein matched the initial spectrum perfectly in the visible region, indicating reversible reaction of both T4moC and the redox mediators. We previously showed that autoxidation of reduced T4moC generated superoxide (*30*). The complete recovery of the optical spectrum indicates that formation of superoxide by a single turnover does not damage the [2Fe-2S] cluster in T4moC. This apparent stability contrasts with the destructive reactions of superoxide with the iron−sulfur clusters in the dehydratase enzyme family (*51*) and in the SoxR (*52*) and FNR (*53*) regulatory proteins.

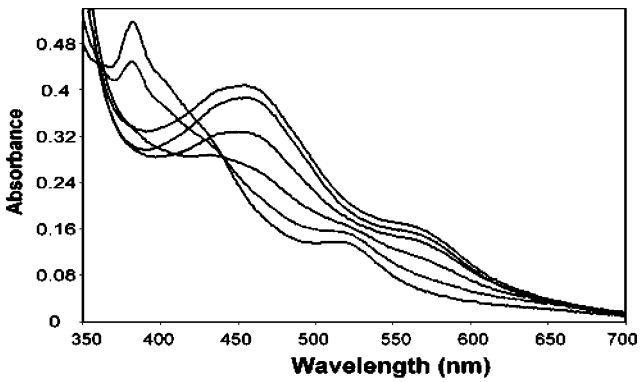

FIGURE 2: Selected optical spectra obtained from a redox titration of T4moC. All spectra were baseline corrected to have zero absorbance at 800 nm. The absorbance band at 566 nm was used for quantification. From the oxidized state (spectrum with $A_{566} = 0.16$), the redox potentials of the individual spectra shown were $+86$, -92, -136, -174, -213, and -275 mV versus the normal hydrogen electrode.

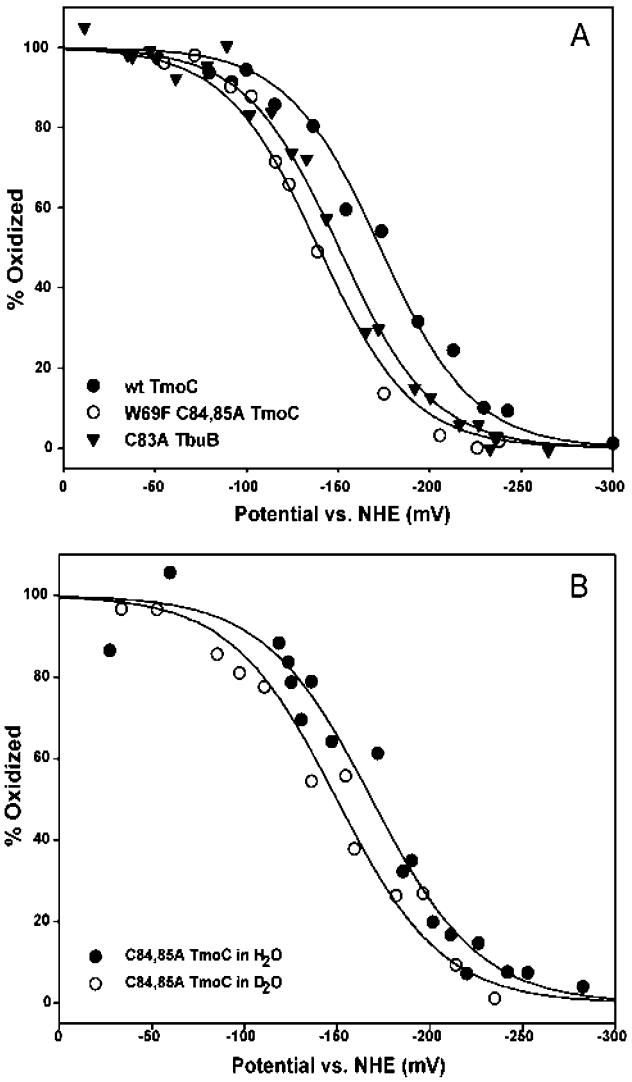

FIGURE 3: Analysis of the redox titrations of T4moC and related proteins. The solid lines are nonlinear least-squares fits of the experimental data using eq 1 with n fixed at 1.0. (A) Titrations of T4moC (filled circles), C83A TbuB (open circles), and W69F C84/C85A T4moC (filled triangles). (B) Titrations of C84A/C85A T4moC in H_2O (filled circles) and D_2O (open circles).

Exchangeable hydrogen bonds to the [2Fe-2S] cluster of T4moC have been established by our previous paramagnetic NMR studies (*43*). As an increase in the strength of hydrogen bonding is postulated to increase the redox potential of a hydrogen-bonded [2Fe-2S] cluster (*17*), the exchange of deuterium for the amide hydrogens should also raise the redox potential. Figure 3B and Table 2 show that titration of C84A/C85A T4moC in 86% D_2O (v/v in the final sample) gave a $+23$ mV shift as compared to the redox potential of the same protein preparation determined in H_2O. This modest shift supports the overall contribution of hydrogen bonding in establishing the redox potential of the [2Fe-2S] cluster. However, as D_2O can have other effects on protein structure and function, such as stabilizing protein folding (*54*), strengthening hydrophobic interactions (*55*), and changing reaction rates, this finding was not further examined.

Saturation Mutagenesis of T4moC W69. The X-ray structures of T4moC and NDO show that a Trp residue is located adjacent to the [2Fe-2S] cluster (*22*, *56*), and an analogous Trp residue is found in the primary sequences of

Table 2: Results of Potentiostatic Redox Titrations of T4moC and Related Rieske Proteins

ferredoxin	E_m[a,b] (mV)	n[c]	ref
T4moC	−173 (4)	0.8 (0.1)	this work
C84/85A T4moC	−169 (6)	0.9 (0.2)	this work
W69F C84/85A T4moC	−139 (4)	1.3 (0.1)	this work
C83A TbuB	−150 (3)	1.1 (0.1)	this work
C84/85A T4moC in D_2O[d]	−150 (7)	0.7 (0.1)	this work
BphF	−157 (2)		*25*
Tt	+161 (4)		*48*
CarAc	−169 (4)		*19*

[a] Reactions were performed at room temperature in 150 mM MOPS, pH 7.0, containing 200 mM KCl and 40 μM redox mediators. [b] Results obtained for least-squares fitting using eq 1 with $n = 1.0$. Error values in parentheses represent two standard deviations. [c] Result obtained from fitting using eq 1 when both E_m and n were allowed to vary. The E_m values determined were within the error shown. [d] Titration performed in buffer containing 86% D_2O (v/v).

Table 3: Complementation of T4MO by T4moC Isoforms and Other Rieske-Type Ferredoxins

ferredoxin	k_{cat} (s^{-1})[a]	K_M (μM)[b]	k_{cat}/K_M (μM^{-1} s^{-1})	coupling efficiency (%)[c]
T4moC[d]	2.9 (0.2)	2.4 (0.4)	1.2	101 (13)
C84A/C85A T4moC	2.6 (0.1)	2.3 (0.2)	1.1	101 (2)
W69F T4moC[f]	0.5 (0.04)	41 (6)	0.01	46 (0.1)
D82A/D83A T4moC[e]	2.3 (0.2)	8 (2)	0.29	
R65A T4moC[e]	3.2 (0.2)	19 (4)	0.17	
TbuB	2.9 (0.2)	21 (2)	0.14	85 (5)
BphF	no activity detected			
Tt	no activity detected			

[a] Apparent k_{cat} values reported relative to the concentration of an $\alpha\beta\gamma$ protomer of T4moH. [b] Apparent K_M values determined using the indicated ferredoxin as the variable substrate and all other required constituents of the catalytic system at fixed, optimized, or saturating concentrations. [c] Coupling efficiency was calculated as the fraction of nanomoles of *p*-cresol produced relative to the nanomoles of NADH consumed (*30*). [d] The values determined as part of this study are consistent with those reported previously (*30*). [e] Values for T4moC determined on the same day with the same T4MO protein preparations were $K_M = 4.3$ (0.8) μM and $k_{cat} = 3.3$ (0.2) s^{-1}. [f] The W69Y variant gave ~20% activity in vivo, similar to the W69F variant, and was not further characterized.

TbuB and other diiron enzyme Rieske-type ferredoxins such as toluene/*o*-xylene monooxygenase ferredoxin (*57*). In T4moC, the position of this Trp residue helps to displace the Pro loop ~8 Å away from the [2Fe-2S] cluster (e.g., see Figure 3 of ref *22*). In contrast, many other Rieske proteins have a small residue in the comparable position, which allows the Pro loop to lie closer to the [2Fe-2S] cluster. For example, BphF and Tt have a glycine residue in this position (Figure 1), while AO [+130 mV (*58*)] and the spinach b_6f oxidase [+319 (*59*)] have either Thr or Ser in this position. In these latter proteins, the hydroxyl groups are hydrogen-bonded to the [2Fe-2S] cluster and contribute to the elevated redox potential (*50*, *60*).

A saturation mutagenesis of T4moC W69 was conducted to determine whether any other residue could provide function at this position. Other than the W69F variant, for which kinetic parameters are shown in Table 3, and W69Y, for which kinetic parameters were judged comparable to W69F in preliminary characterizations and not further investigated, no other residue at the position of W69 yielded

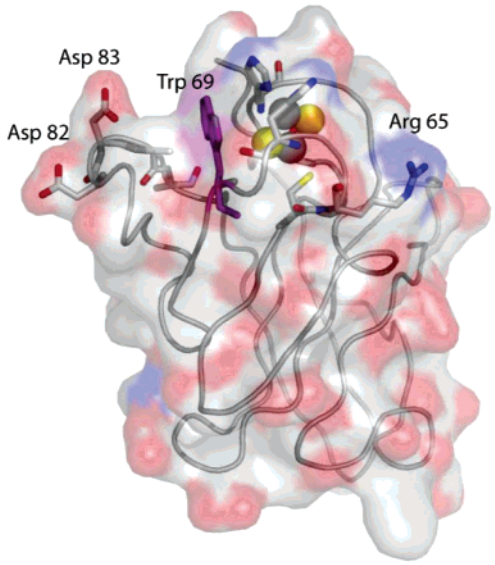

FIGURE 4: Representation of the T4moC structure showing the location of R65 (blue), W69 (purple), and D82 and D83 (red) in relation to the [2Fe-2S] cluster. In the orientation shown here, C84A and C85A are on the opposite side of the molecule, behind D82 and D83, and not visible.

greater than 1% of the catalytic activity of the natural isoform as judged by in vivo assays.[2]

The purified W69F isoform had an optical absorption spectrum typical for a Rieske ferredoxin (λ_{max} at 456 nm) and $A_{280}/A_{456} \approx 5$, consistent with full incorporation of the [2Fe-2S] cluster. The potential determined for W69F C84A/C85A T4moC was −139 ± 4 mV, a +30 mV shift relative to C84A/C85A T4moC. A steady-state kinetic analysis of the purified W69F isoform (see Table 2) showed an ~80% decrease in k_{cat} and a 20-fold increase in K_M relative to the natural protein (120-fold decrease in k_{cat}/K_M). These altered kinetic parameters were also associated with a substantial loss of coupling efficiency. Thus alteration of a conserved aromatic residue immediately adjacent to the [2Fe-2S] cluster influenced the redox potential, the k_{cat}, and the apparent K_M of W69F T4moC.

Mutagenesis of Asp82 and Asp83. Figure 4 shows the location of D82 and D83 on the one surface of T4moC. TbuB contains glycine residues in the positions of these aspartate residues but retains many others that are similar in size, charge, and polarity when compared to T4moC, including W69. In contrast, BphF has many different residue types situated on the comparable surface around the [2Fe-2S] cluster, suggesting that this surface of the protein may be important in catalytic specificity for the different Rieske-type ferredoxins.

Table 3 shows that D82A/D83A T4moC has both an ~30% decrease in k_{cat} and an ~3-fold increase in K_M relative to T4moC. These changes mirror the changes in both k_{cat} and K_M observed for W69F T4moC (Table 2). It is noted that these three residues reside on the same surface of T4moC

[2] The W69A variant, which was unstable in preparation and exhibited only ~1% activity in vivo relative to the natural protein, was purified in order to investigate [2Fe-2S] incorporation. In this case, only a low yield of the protein was obtained, and the $A_{280}/A_{456} \approx 10$ observed from the purified W69A variant suggested that instability of the [2Fe-2S] cluster was the primary reason for the lack of activity.

and so may reasonably have coordinated effects on catalysis, particularly if they participate in forming a protein−protein interface.

Mutagenesis of Arg65. Figure 4 also shows the location of R65 of T4moC. R65 combines with H67 to form a basic patch on the upper surface of T4moC. These two residues are on the opposite side of the [2Fe-2S] cluster from W69, D82, and D83. TbuB also contains an arginine residue comparable to R65 of T4moC, while BphF contains a serine residue at this position. Table 3 shows that R65A T4moC has an ∼10-fold increase in apparent K_M as compared to T4moC but no change in the apparent k_{cat}.

Catalytic Complementation Studies. T4moC was individually substituted with other Rieske ferredoxins in order to assess the ability of these structural homologues to complement the catalytic reaction of the purified T4MO complex. Table 3 shows the results obtained from steady-state v versus [S] analysis, where the rate of *p*-cresol formation was determined with the added Rieske ferredoxin acting as the variable substrate (*30*).

Reconstitution with the Rieske-type ferredoxin TbuB (from the related diiron monooxygenase complex) gave k_{cat} identical to T4moC but had k_{cat}/K_M decreased by a factor of ∼8, arising from a larger apparent K_M value. These results are strongly suggestive that minor changes in redox potential of the alternate ferredoxin (+23 mV) did not sufficiently slow electron transfer relative to other steps of catalysis that are rate-determining even as apparent binding interactions were decreased. For reconstitution with TbuB, the coupling between NADH utilization and *p*-cresol formation was only slightly decreased from reactions with T4moC, further supporting the conclusion that interactions required to maintain catalysis are largely retained in the heterologous complex. In contrast, no catalytic activity was detected from either BphF or Tt, even when the alternate ferredoxin was added at a concentration 10-fold above the apparent K_M for T4moC. Upon accounting for the sensitivity of the catalytic assay, the apparent K_M for these nonfunctional alternative ferredoxins would be at least 500-fold higher than the functional homologues. The W69F T4moC had a redox potential similar to TbuB (−139 versus −150 mV, respectively) but, unlike TbuB, had k_{cat}/K_M changed by 120-fold relative to TbuB.

These results demonstrate catalytic specialization of function within the broader group of Rieske ferredoxins. Since TbuB (−150 mV, catalytic complementation), BphF (−157 mV, no catalytic complementation), and W69F T4moC (−139 mV, partial catalytic complementation) have redox potentials close to T4moC (−173 mV), the difference in catalytic properties of the two alternative ferredoxins cannot be uniquely assigned to the thermodynamics of electron transfer. Thus specificity most likely arises from shape or electrostatic differences in protein structure that affect the formation of an efficient electron transfer complex.

DISCUSSION

There is overwhelming evidence for structural similarity within the Rieske-type ferredoxin family. Nevertheless, these proteins also have highly specialized functional capabilities. Here we have shown that only TbuB, the natural ferredoxin most closely related to T4moC, was able to substitute in reconstitution of T4MO activity, evoking broad questions regarding the nature of protein−protein interactions required for efficient electron transfer between Rieske-type ferredoxins and their cognate electron acceptors.

Redox Properties. Among the Rieske proteins studied here, Tt has seven hydrogen bonds to the [2Fe-2S] cluster and a high redox potential ($E_m \approx +150$ mV, ∼300 mV higher than the other ferredoxins examined) and thus may not be a sufficiently strong reductant for the non-heme iron clusters present in the dioxygenase and monooxygenase acceptors [for example, the T4moH diiron cluster (*24*) has strong similarity to the methane monooxygenase hydroxylase diiron cluster, which has $E_m \approx -115$ mV (*61*)]. Furthermore, Tt also has marked differences in the surface charge and loop structure when compared with T4moC, perhaps interfering with electrostatic or steric interactions required to form an effective electron transfer complex. In contrast, BphF has a redox potential ($E_m = -157$ mV) similar to T4moC ($E_m = -173$ mV) and TbuB ($E_m = -150$ mV). Consequently, thermodynamic barriers to substitution of BphF for electron transfer into the T4MO complex would seemingly be less. However, no catalysis was observed with BphF. By comparison, catalytic complementation was obtained with TbuB and a variety of mutated T4moC isoforms, where the redox potential was raised by up to 30 mV. These cumulative results implicate specific features of protein−protein interactions in catalytic specificity.

Surfaces Charge and Steric Features. At pH 7.0, T4moC has a total protein charge of −13.9, TbuB has a charge of −8.9, and BphF has a charge of −7.0. By comparing the structures of T4moC and BphF, it is clear that T4moC has a higher negative charge on the surface, particularly on the localized protein surface shown in Figure 5. Furthermore, the presence of W69 in T4moC displaces the Pro loop ∼8 Å away from the [2Fe-2S] cluster, so unfavorable electrostatic and steric interactions might prevent formation of an effective electron transfer complex even as the similarity of redox potentials argue in favor of electron transfer. As electrostatic pairing between electron donor and acceptor has known contributions to forming effective electron transfer partners (*1*, *2*, *62*−*64*), the widely distributed residue changes between T4moC and BphF may also partially contribute to the differences in catalytic complementation through altered binding.

Structural modeling of TbuB, a close evolutionary variant of T4moC, suggests that both surface charge and molecular shape (including conservation at R65 and W69) will be largely conserved in these two ferredoxins. Notably, TbuB was able to complement T4MO activity with k_{cat} comparable to T4moC, while the change in k_{cat}/K_M arose from a small increase in apparent K_M. This result is consistent with minor alterations in the protein−protein interactions required for electron transfer, which may also reflect the differences in total charge calculated for these two proteins (−13.9 for T4moC versus −8.9 for TbuB). Thus conservation of W69 in T4moC and TbuB, which is predicted to result in a similar structure near the Pro loop, allows for efficient complementation. In contrast, complementation with BphF may first be disrupted by steric considerations, with electrostatics having a secondary role.

Redox Potential of T4moC. A detailed examination of the relationship of W69 to the [2Fe-2S] cluster (see Figure 6)

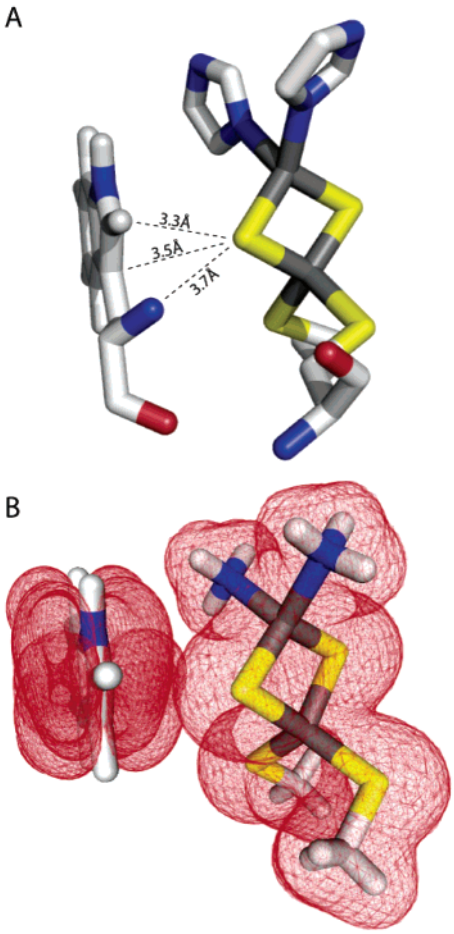

FIGURE 5: Orbital contacts between W69 of T4moC and the [2Fe-2S] cluster. Carbon atoms are in light gray, nitrogens are in blue, oxygens are in red, hydrogens are in white, sulfurs are in yellow, and irons are in dark gray. (A) Stick representation of W69, the [2Fe-2S] cluster, and its ligands from the X-ray crystal structure of T4moC (*22*). Distances between two carbon atoms of the indole ring and the backbone amide nitrogen of W69 and an inorganic sulfide of the [2Fe-2S] cluster are shown. (B) Model of the interaction between the indole ring of W69 and the Rieske cluster shown in the same orientation as in panel A. The surface shows the combination of six molecular orbitals with primarily carbon or nitrogen p_z orbital character on the indole ring and the electron density calculated for the truncated Rieske cluster model. The molecular orbitals and electron density were calculated with the electronic structure software package ORCA (*34*).

reveals that the π-orbitals of the aromatic ring are juxtaposed with an inorganic sulfide of the [2Fe-2S] cluster. In particular, two carbon atoms of the ring are 3.3 and 3.5 Å from the sulfide, closer than any hydrogen bond donating atom, thus creating a localized region of high electron density with a negative dipole moment directly adjacent to the [2Fe-2S] cluster. In effect, this places an "anti-hydrogen bond" on the [2Fe-2S] cluster by donation of electron density instead of removing it via an intervening hydrogen atom. This feature may contribute to the lower than anticipated redox potential for T4moC. The substitution of phenylalanine may retain an aromatic system in the vicinity of the [2Fe-2S] cluster, and we therefore propose that this is a conservative mutation in terms of the effect on the electronic structure of the [2Fe-2S] cluster.

W69 aligns structurally (Figure 1) with the hydrogen-bonding threonine and serine residues in other Rieske ferredoxins which have been previously shown to raise the [2Fe-2S] redox potential by up to ~130 mV (*45*). There is an ~+30 mV shift in W69F C84A/C85A T4moC as compared to T4moC, which is consistent with the observation that changes at this position can modulate the Rieske cluster redox potential. The ability of other aromatic amino acid side chains to allow catalytic complementation at the position corresponding to W69 in T4moC is supported by the observation that the Rieske domain of 2-oxoquinoline 8-monooxygenase has F110 in the same spatial position relative to the [2Fe-2S] cluster [PDB code 1z03 (*65*)].

In 2-oxoquinoline 8-monooxygenase, F110-N is 3.50 Å from a μ-sulfide with an angle of 163° between F110-N, the riding hydrogen, and the μ-sulfide. Other atoms of F110 close to the μ-sulfide include CB at 3.66 Å, CG at 3.67 Å, and CD1 at 3.32 Å. The distances are comparable to the following atoms of W69 and μ-sulfide in T4moC: N at 3.66 Å (angle 163°), CB at 3.81 Å, CG at 3.50 Å, CD1 at 3.32 Å, and NE1 at 3.86 Å. Electron density at the CD1 position of a phenyl ring is calculated to be lower than for either the CG or CD1 positions of an indole ring (*34*), suggesting how closely approaching aromatic residues might also contribute to the differences in redox potential measured for W69 and W69F T4moC (Table 2). Other factors may also contribute to the lowered redox potential seen for T4moC relative to our initial estimate of ~0 mV upon the basis of the hydrogen-bonding pattern observed in the crystal structure (*22*) and the correlation provided in Figure 5, Supporting Information of ref *17*. Thus small changes in the distance and angle of hydrogen bonds to the cluster may play a role (*48*), and access of water to the cluster has also been invoked by others (*25*). In particular, the backbone amide of W69 is the farthest from the cluster, with a distance of ~3.7 Å (*29*), while changes in the size of the indole versus phenyl ring or methyl group may change water access, redox potential, and stability of the [2Fe-2S] cluster.[2] Furthermore, the large number of glutamate and aspartate residues on the surface of T4moC also contributes to a global electrostatic environment surrounding the cluster that is more negative compared to other Rieske ferredoxins, potentially lowering the redox potential.

Models for Protein Interactions As Indicated by Rieske Ferredoxin Structures. Recently, Poulos and co-workers considered experimental and docking results on the interaction of putidaredoxin with putidaredoxin reductase (*1*) by reference to the X-ray structure of the ferredoxin:$NADP^+$ reductase complex (*64*). This comparison helped to illustrate reasonable possibilities for the putidaredoxin:putidaredoxin reductase complex.

Figure 6 shows crystallographically defined interactions between the subunits of the multimeric enzymes naphthalene dioxygenase (Figure 6A) and arsenite oxidase (Figure 6C). These structures show that different surfaces of the Rieske protein domain can provide essential protein−protein contacts. In each case, the predicted electron transfer path involves the His ligands of the [2Fe-2S] cluster and the other redox site [non-heme Fe cluster, H208 and D205, Figure 6A (*56*); [3Fe-4S] cluster and molybdopterin, Figure 6C (*11*, *58*)]. The importance of the interaction surface is demonstrated for the [2Fe-2S] cluster of anthranilate dioxygenase, an enzyme related to naphthalene dioxygenase, which undergoes a −100 mV shift upon mutation of the aspartate residue that bridges the Rieske cluster and mononuclear iron site (*66*), and by mutagenesis studies of the Asp residue that

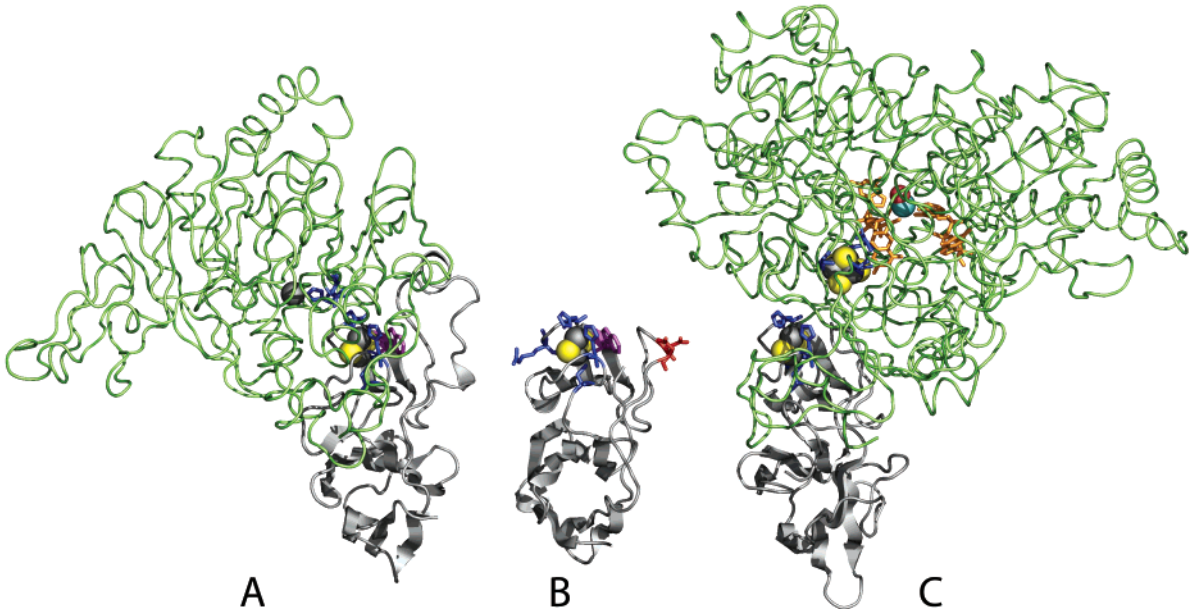

FIGURE 6: Electron transfer interfaces of enzymes involving Rieske-type ferredoxin domains. The [2Fe-2S] clusters of each structure were aligned using the PyMOL pair_fit routine. (A) Naphthalene dioxygenase (1NDO). The Rieske domain of one polypeptide chain is shown as a gray ribbon, and the remainder of the chain is shown in cyan. The adjacent subunit is shown as a green ribbon along with the position of the mononuclear non-heme iron site. The tryptophan residues discussed for T4moC and the Rieske domain naphthalene dioxygenase are shown in purple stick representation. (B) T4moC is shown as a ribbon trace in the same orientation as in panel A. (C) Arsenite oxidase (1g8k). The Rieske-containing subunit is shown as a gray ribbon. The adjacent subunit is shown in blue along with the position of the [3Fe-4S] cluster and molybdopterin cofactors.

bridges between the [2Fe-2S] cluster and the mononuclear iron site in phthalate dioxygenase (*67*, *68*). Studies of 2-oxoquinoline 8-monooxygenase also show that changes in redox state of the Rieske center can affect ligation geometry at a distal mononuclear Fe site (*65*).

We wondered whether the structures of Rieske domains shown in electron transfer configurations in Figure 6 might lend insight into the possible nature of the interactions of T4moC with other proteins of the T4MO complex. Figure 6B shows the ribbon trace of T4moC in the same orientation as the other two Rieske domains in Figure 6, along with the position of W69 (purple) and the two closely spaced residues D82 and D83 on one side of the [2Fe-2S] cluster and R65 on the other side. The work presented here shows that R65A impairs steady-state catalysis by decreasing the apparent K_M for T4moC in the steady-state reaction while having no effect on k_{cat}. In contrast, mutations at W69, D82, and D83 influence catalysis by causing a decrease in k_{cat} and an increase in the apparent K_M. We hypothesize that two different surfaces may potentially be used when T4moC interacts with either an electron donor (T4moF, NADH oxidoreductase) or an electron acceptor (T4moH, diiron hydroxylase). Recent fluorescence anisotropy studies suggest that T4moC and T4moD also interact (*69*), perhaps through one of these putative electron transfer surfaces. How these surface mutations can influence steady-state catalysis is not clear. Nevertheless, the present results indicate the importance of two regions flanking the [2Fe-2S] cluster of T4moC for catalysis, and both of these regions are represented in crystal structures in other enzymes.

CONCLUSION

The studies reported here emphasize the remarkable degree of specificity that ferredoxins, and in particular Rieske ferredoxins, have in interactions with their electron transfer partners. This work indicates that differences in the protein fold topology and the distribution of protein surface charge are important contributors to specialization of Rieske protein function. By detailed comparisons and further mutagenesis, we have identified two regions that may contribute to the catalytic interfaces formed between T4moC and other components of the four-protein enzyme complex. The further identification of specific contacts and their influence on catalysis are of continuing interest.

ACKNOWLEDGMENT

The authors thank Dr. James A. Fee (The Scripps Research Institute) and Prof. Lindsay Eltis (University of British Columbia) for generous gifts of purified *T. thermophilus* Rieske protein and BphF used in this work, Dr. Glen Hinckley and Dr. Perry Frey (University of Wisconsin) for use of the potentiostat and helpful insights, and Dr. Thomas Brunold (University of Wisconsin) for help with electronic structure calculations using ORCA.

REFERENCES

1. Kuznetsov, V. Y., Blair, E., Farmer, P. J., Poulos, T. L., Pifferitti, A., and Sevrioukova, I. F. (2005) The putidaredoxin reductase-putidaredoxin electron transfer complex: theoretical and experimental studies, *J. Biol. Chem. 280*, 16135−16142.
2. Tollin, G., Cheddar, G., Watkins, J. A., Meyer, T. E., and Cusanovich, M. A. (1984) Electron transfer between flavodoxin semiquinone and *c*-type cytochromes: correlations between electrostatically corrected rate constants, redox potentials, and surface topologies, *Biochemistry 23*, 6345−6349.
3. Ludden, P. W., Okon, Y., and Burris, R. H. (1978) The nitrogenase system of *Spirillum lipoferum*, *Biochem. J. 173*, 1001−1003.
4. Johnson, D. C., Dean, D. R., Smith, A. D., and Johnson, M. K. (2005) Structure, function, and formation of biological iron-sulfur clusters, *Annu. Rev. Biochem. 74*, 247−281.

5. Stephens, P. J., Jollie, D. R., and Warshel, A. (1996) Protein control of redox potentials of iron-sulfur proteins, *Chem. Rev. 96*, 2491−2514.
6. Trumpower, B. L., and Gennis, R. B. (1994) Energy transduction by cytochrome complexes in mitochondrial and bacterial respiration: the enzymology of coupling electron transfer reactions to transmembrane proton translocation, *Annu. Rev. Biochem. 63*, 675−716.
7. Berry, E. A., Guergovas-Kuras, M., Huang, L. S., and Crofts, A. R. (2000) Structure and function of cytochrome *bc* complexes, *Annu. Rev. Biochem. 69*, 1005−1075.
8. Mason, J. R., and Cammack, R. (1992) The electron-transport proteins of hydroxylating bacterial dioxygenases, *Annu. Rev. Microbiol. 46*, 277−305.
9. Harayama, S., Kok, M., and Neidle, E. L. (1992) Functional and evolutionary relationships among diverse oxygenases, *Annu. Rev. Microbiol. 46*, 565−601.
10. Harborne, N. R., Griffiths, L., Busby, S. J., and Cole, J. A. (1992) Transcriptional control, translation and function of the products of the five open reading frames of the *Escherichia coli nir* operon, *Mol. Microbiol. 6*, 2805−2813.
11. Ellis, P. J., Conrads, T., Hille, R., and Kuhn, P. (2001) Crystal structure of the 100 kDa arsenite oxidase from Alcaligenes faecalis in two crystal forms at 1.64 Å and 2.03 Å, *Structure 9*, 125−132.
12. Gibson, D. T., and Parales, R. E. (2000) Aromatic hydrocarbon dioxygenases in environmental biotechnology, *Curr. Opin. Biotechnol. 11*, 236−43.
13. Leahy, J. G., Batchelor, P. J., and Morcomb, S. M. (2003) Evolution of the soluble diiron monooxygenases, *FEMS Microbiol. Rev. 27*, 449−479.
14. Batie, C. J., Ballou, D. P., and Correll, C. C. (1992) Phthalate dioxygenase reductase and related flavin-iron-sulfur containing electron transferases, in *Chemistry and Biochemistry of the Flavoenzymes* (Mueller, F., Ed.) pp 543−556, CRC Press, Boca Raton, FL.
15. Colbert, C. L., Couture, M. M., Eltis, L. D., and Bolin, J. T. (2000) A cluster exposed: structure of the Rieske ferredoxin from biphenyl dioxygenase and the redox properties of Rieske Fe-S proteins, *Structure 8*, 1267−1278.
16. Link, T. (1999) The structures of Rieske and Rieske-type proteins, *Adv. Inorg. Chem. 47*, 83−157.
17. Hunsicker-Wang, L. M., Heine, A., Chen, Y., Luna, E. P., Todaro, T., Zhang, Y. M., Williams, P. A., McRee, D. E., Hirst, J., Stout, C. D., and Fee, J. A. (2003) High-resolution structure of the soluble, respiratory-type Rieske protein from *Thermus thermophilus*: analysis and comparison, *Biochemistry 42*, 7303−7317.
18. Link, T. A., and Iwata, S. (1996) Functional implications of the structure of the "Rieske" iron-sulfur protein of bovine heart mitochondrial cytochrome bc_1 complex, *Biochim. Biophys. Acta 1275*, 54−60.
19. Nam, J. W., Noguchi, H., Zui, Fujimoto, Mizuno, H., Ashikawa, Y., Abo, M., Fushinobu, S., Kobashi, N., Wakagi, T., Iwata, K., Yoshida, T., Habe, H., Yamane, H., Omori, T., and Nojiri, H. (2005) Crystal structure of the ferredoxin component of carbazole 1,9a-dioxygenase of *Pseudomonas resinovorans* strain CA10, a novel Rieske non-heme iron oxygenase system, *Proteins: Struct., Funct., Bioinf. 58*, 779−789.
20. Bonisch, H., Schmidt, C. L., Schafer, G., and Ladenstein, R. (2002) The structure of the soluble domain of an archaeal Rieske iron-sulfur protein at 1.1 Å resolution, *J. Mol. Biol. 319*, 791−805.
21. Iwata, S., Saynovits, M., Link, T. A., and Michel, H. (1996) Structure of a water soluble fragment of the "Rieske" iron-sulfur protein of the bovine heart mitochondrial cytochrome bc_1 complex determined by MAD phasing at 1.5 Å resolution, *Structure 4*, 567−579.
22. Moe, L., Bingman, C. A., Wesenberg, G. E., Phillips, G. N., and Fox, B. G. (2006) Structure of T4moC, the Rieske-type ferredoxin component of toluene 4-monooxygenase, *Acta Crystallogr., Sect. D: Biol. Crystallogr. 62*, 476−482.
23. Whited, G. M., and Gibson, D. T. (1991) Toluene 4-monooxygenase, a three component enzyme system that catalyzes the oxidation of toluene to *p*-cresol in *Pseudomonas mendocina KR1*, *J. Bacteriol. 173*, 3010−3016.
24. Pikus, J. D., Studts, J. M., Achim, C., Kauffmann, K. E., Münck, E., Steffan, R. J., McClay, K., and Fox, B. G. (1996) Recombinant toluene 4-monooxygenase: Catalytic and Mössbauer studies of the purified diiron and Rieske components of a four-protein complex, *Biochemistry 35*, 9106−9119.
25. Couture, M. M., Colbert, C. L., Babini, E., Rosell, F. I., Mauk, A. G., Bolin, J. T., and Eltis, L. D. (2001) Characterization of BphF, a Rieske-type ferredoxin with a low reduction potential, *Biochemistry 40*, 84−92.
26. Olsen, R. H., Kukor, J. J., and Kaphammer, B. (1994) A novel toluene-3-monooxygenase pathway cloned from *Pseudomonas pickettii* PK01, *J. Bacteriol. 176*, 3749−3756.
27. Pikus, J. D., Studts, J. M., McClay, K., Steffan, R. J., and Fox, B. G. (1997) Changes in the regiospecificity of aromatic hydroxylation produced by active site engineering in the diiron enzyme toluene 4-monooxygenase, *Biochemistry 36*, 9283−9289.
28. Studts, J. M., and Fox, B. G. (1999) Application of fed-batch fermentation to the preparation of isotopically labeled or selenomethionine-labeled proteins, *Protein Expression Purif. 16*, 109−119.
29. Xia, B., Pikus, J. D., Xia, W., McClay, K., Steffan, R. J., Chae, Y. K., Westler, W. M., Markley, J. L., and Fox, B. G. (1999) Detection and classification of hyperfine-shifted ^{1}H, ^{2}H, and ^{15}N resonances of the Rieske ferredoxin component from toluene 4-monooxygenase, *Biochemistry 38*, 727−739.
30. Mitchell, K. H., Studts, J. M., and Fox, B. G. (2002) Combined participation of effector protein binding and hydroxylase active site residues provide toluene 4-monooxygenase regiospecificity, *Biochemistry 41*, 3176−3188.
31. Hinckley, G. T., and Frey, P. A. (2006) An adaptable spectroelectrochemical titrator: The midpoint reduction potential of the iron-sulfur center in lysine 2,3-aminomutase, *Anal. Biochem. 349*, 103−111.
32. Bailey, S. I., and Ritchie, I. M. (1985) A cyclic voltammetric study of the aqueous electrochemistry of some quinines, *Electrochim. Acta 30*, 3−12.
33. Clark, W. M. (1960) *Oxidation-reduction potentials of organic systems*, Williams and Wilkins, Baltimore, MD.
34. Neese, F. (2004) Orca-An ab initio, Density Functional, and Semiempirical Program Package, Version 2.4, revision 2, July 2004. Max-Planck-Institut für Bioanorganische Chemie, Mülheim, Germany.
35. Schäfer, A., Horn, H., and Ahlrichs, R. (1992) Fully optimized contracted Gaussian-basis sets for atoms Li to Kr, *J. Chem. Phys. 97*, 2571−2577.
36. Becke, A. (1993) A new mixing of Hartree-Fock and local density-functional theories, *J. Chem. Phys. 98*, 1372−1377.
37. Lee, C., Yang, W., and Parr, R. (1988) Development of the Colle-Salvetti correlation-energy formula into a functional of the electron density, *Phys. Rev. B 37*, 785−789.
38. Laaksonen, L. (1992) A graphics program for the analysis and display of molecular dynamics trajectories, *J. Mol. Graphics 10*, 33−34.
39. Chen, J., Anderson, J. B., DeWeese-Scott, C., Fedorova, N. D., Geer, L. Y., He, S., Hurwitz, D. I., Jackson, J. D., Jacobs, A. R., Lanczycki, C. J., Liebert, C. A., Liu, C., Madej, T., Marchler-Bauer, A., Marchler, G. H., Mazumder, R., Nikolskaya, A. N., Rao, B. S., Panchenko, A. R., Shoemaker, B. A., Simonyan, V., Song, J. S., Thiessen, P. A., Vasudevan, S., Wang, Y., Yamashita, R. A., Yin, J. J., and Bryant, S. H. (2003) MMDB: Entrez's 3D-structure database, *Nucleic Acids Res. 31*, 474−477.
40. Lambert, C., Leonard, N., De, Bolle, X., and Depiereux, E. (2002) ESyPred3D: Prediction of proteins 3D structures, *Bioinformatics 18*, 1250−1256.
41. Baker, N. A., Sept, D., Joseph, S., Holst, M. J., and McCammon, J. A. (2001) Electrostatics of nanosystems: application to microtubules and the ribosome, *Proc. Natl. Acad. Sci. U.S.A. 98*, 10037−10041.
42. Holst, M., and Saied, F. (1995) Numerical solution of the nonlinear Poisson-Boltzmann equation: Developing more robust and efficient methods, *J. Comput. Chem. 16*, 337−364.
43. Skjeldal, L., Peterson, F. A., Doreleijers, J. F., Moe, L. A., Pikus, J. D., Volkman, B. F., Westler, W. M., Markley, J. L., and Fox, B. G. (2004) Solution structure of T4moC, the Rieske ferredoxin component of the toluene 4-monooxygenase complex, *J. Biol. Inorg. Chem. 9*, 945−953.
44. Nam, J. W., Nojiri, H., Yoshida, T., Habe, H., Yamane, H., and Omori, T. (2001) New classification system for oxygenase components involved in ring-hydroxylating oxygenations, *Biosci., Biotechnol., Biochem. 65*, 254−263.
45. Denke, E., Merbitz-Zahradnik, T., Hatzfeld, O. M., Snyder, C. H., Link, T. A., and Trumpower, B. L. (1998) Alteration of the midpoint potential and catalytic activity of the Rieske iron-sulfur

protein by changes of amino acids forming hydrogen bonds to the iron-sulfur cluster, *J. Biol. Chem. 273*, 9085−9093.
46. Schröter, T., Hatzfield, O. M., Gemeinhardt, S., Korn, M., Friedrich, T., Ludwig, B., and Link, T. A. (1998) Mutational analysis of residues forming hydrogen bonds in the Rieske [2Fe-2S] cluster of the cytochrome bc_1 complex in *Paracoccus denitrificans*, *Eur. J. Biochem. 255*, 100−106.
47. Klingen, A. R., and Ullmann, G. M. (2004) Negatively charged residues and hydrogen bonds tune the ligand histidine pK_a values of Rieske iron-sulfur proteins, *Biochemistry 43*, 12383−12389.
48. Zu, Y., Couture, M. M., Kolling, D. R., Crofts, A. R., Eltis, L. D., Fee, J. A., and Hirst, J. (2003) Reduction potentials of Rieske clusters: importance of the coupling between oxidation state and histidine protonation state, *Biochemistry 42*, 12400−12408.
49. Brugna, M., Nitschke, W., Asso, M., Guigliarelli, B., Lemesle-Meunier, D., and Schmidt, C. (1999) Redox components of cytochrome *bc*-type enzymes in acidophilic prokaryotes, *J. Biol. Chem. 274*, 16766−16772.
50. Carrell, C. J., Zhang, H., Cramer, W. A., and Smith, J. L. (1997) Biological identity and diversity in photosynthesis and respiration: structure of the lumen-side domain of the chloroplast Rieske protein, *Structure 5*, 1613−1625.
51. Flint, D. H., Tuminello, J. F., and Emptage, M. H. (1993) The inactivation of Fe-S cluster containing hydro-lyases by superoxide, *J. Biol. Chem. 268*, 22369−22376.
52. Ding, H., and Demple, B. (1998) Thiol-mediated disassembly and reassembly of [2Fe-2S] clusters in the redox-regulated transcription factor SoxR, *Biochemistry 37*, 17280−17286.
53. Sutton, V. R., Stubna, A., Patschkowski, T., Munck, E., Beinert, H., and Kiley, P. J. Superoxide destroys the $[2Fe\text{-}2S]^{2+}$ cluster of FNR from *Escherichia coli*, *Biochemistry 43*, 791−798.
54. Cardinale, G. J., and Abeles, R. H. (1968) Purification and mechanism of action of proline reacemase, *Biochemistry 7*, 3970−3978.
55. Itzhaki, L. S., and Evans, P. A. (1996) Solvent isotope effects on the refolding kinetics of hen egg-white lysozyme, *Protein Sci. 5*, 140−146.
56. Kauppi, B., Lee, K., Carredano, E., Parales, R. E., Gibson, D. T., Eklund, H., and Ramaswamy, S. (1998) Structure of an aromatic-ring-hydroxylating dioxygenase-naphthalene 1,2-dioxygenase, *Structure 6*, 571−586.
57. Bertoni, G., Bolognesi, F., Galli, E., and Barbieri, P. (1996) Cloning of the genes for and characterization of the early stages of toluene catabolism in *Pseudomonas stutzeri* OX1, *Appl. Environ. Microbiol. 62*, 3704−3711.
58. Hoke, K., Cobb, N., Armstrong, F., and Hille, R. (2004) Electrochemical studies of arsenite oxidase: an unusual example of a highly cooperative two-electron molybdenum center, *Biochemistry 43*, 1667−1674.
59. Zhang, H., Carrell, C., Huang, D., Sled, V., Ohnishi, T., Smith, J., and Cramer, W. (1996) Characterization and crystallization of the lumen side domain of the chloroplast Rieske iron-sulfur protein, *J. Biol. Chem. 271*, 31360−31366.
60. Link, T. A., Hatzfield, O. M., Unalkat, P., Shergill, J. K., Cammack, R., and Mason, J. R. (1996) Comparison of the "Rieske" [2Fe-2S] center in the bc_1 complex and in bacterial dioxygenases by circular dichroism spectroscopy and cyclic voltammetry, *Biochemistry 35*, 7546−7552.
61. Paulsen, K. E., Liu, Y., Fox, B. G., Lipscomb, J. D., Münck, E., and Stankovich, M. T. (1994) Oxidation-reduction potentials of the methane monooxygenase hydroxylase component from *Methylosinus trichosporium* OB3b, *Biochemistry 33*, 713−722.
62. Martinez-Julvez, M., Medina, M., Hurley, J., Hafezi, R., Brodie, T., Tollin, G., and Gomez-Moreno, C. (1998) Lys75 of *Anabaena* ferredoxin-$NADP^+$ reductase is a critical residue for binding ferredoxin and flavodoxin during electron transfer, *Biochemistry 37*, 13604−13613.
63. Sobrado, P., Lyle, K., Kaul, S., Turco, M., Arabshahi, I., Marwah, A., and Fox, B. (2006) Indentification of the binding region of the [2Fe-2S] ferredoxin in stearoyl-acyl carrier protein desaturase: Insight into the catalytic complex and mechanism of action, *Biochemistry 45*, 4848−4858.
64. Morales, R., Charon, M. H., Kachalova, G., Serre, L., Medina, M., Gomez-Moreno, C., and Frey, M. (2000) A redox-dependent interaction between two electron-transfer partners involved in photosynthesis, *EMBO Rep. 1*, 271−276.
65. Martins, B. M., Svetlitchnaia, T., and Dobbek, H. (2005) 2-oxoquinoline 8-monooxygenase oxygenase component: Active site modulation by Rieske-[2Fe-2S] center oxidation/reduction, *Structure 13*, 817−824.
66. Beharry, Z. M., Eby, D. M., Coulter, E. D., Viswanathan, R., Neidle, E. L., Phillips, R. S., and Kurtz, D. M., Jr. (2003) Histidine ligand protonation and redox potential in the Rieske dioxygenases: role of a conserved aspartate in anthranilate 1,2-dioxygenase, *Biochemistry 42*, 13625−13636.
67. Pinto, A., Tarasev, M., and Ballou, D. P. (2006) Substitutions of the "bridging" aspartate 178 result in profound changes in the reactivity of the Rieske center of phthalate dioxygenase, *Biochemistry 45*, 9032−9041.
68. Tarasev, M., Pinto, A., Kim, D., Elliott, S. J., and Ballou, D. P. (2006) The "bridging" aspartate 178 in phthalate dioxygenase facilitates interactions between the Rieske center and the iron-(II)−mononuclear center, *Biochemistry 45*, 10208−10216.
69. Moe, L., McMartin, L., and Fox, B. (2006) Component interactions and implications for complex formation in the multicomponent toluene 4-monooxygenase, *Biochemistry 45*, 5478−5485.

BI0616145